Cell Host & Microbe
Article

The Antiviral Effector IFITM3 Disrupts Intracellular Cholesterol Homeostasis to Block Viral Entry

Samad Amini-Bavil-Olyaee,[1] Youn Jung Choi,[1,2] Jun Han Lee,[1] Mude Shi,[1] I-Chueh Huang,[3] Michael Farzan,[4] and Jae U. Jung[1,2,*]

[1]Department of Molecular Microbiology and Immunology, Keck School of Medicine
[2]Department of Pharmacology and Pharmaceutical Sciences, School of Pharmacy
University of Southern California, Harlyne J. Norris Cancer Research Tower, 1450 Biggy Street, Los Angeles, CA 90033, USA
[3]College of Natural and Agricultural Sciences, Cell Biology & Neuroscience Biological Science Building, University of California, Riverside, 900 University Avenue, Riverside, CA 92521, USA
[4]Department of Infectious Diseases, The Scripps Research Institute, 130 Scripps Way, Jupiter, FL 33458, USA
*Correspondence: jaeujung@med.usc.edu
http://dx.doi.org/10.1016/j.chom.2013.03.006

SUMMARY

Vesicle-membrane-protein-associated protein A (VAPA) and oxysterol-binding protein (OSBP) regulate intracellular cholesterol homeostasis, which is required for many virus infections. During entry, viruses or virus-containing vesicles can fuse with endosomal membranes to mediate the cytosolic release of virions, and alterations in endosomal cholesterol can inhibit this invasion step. We show that the antiviral effector protein interferon-inducible transmembrane protein 3 (IFITM3) interacts with VAPA and prevents its association with OSBP, thereby disrupting intracellular cholesterol homeostasis and inhibiting viral entry. By altering VAPA-OSBP function, IFITM3 induces a marked accumulation of cholesterol in multivesicular bodies and late endosomes, which inhibits the fusion of intraluminal virion-containing vesicles with endosomal membranes and thereby blocks virus release into the cytosol. Consequently, ectopic expression or depletion of the *VAPA* gene profoundly affects IFITM3-mediated inhibition of viral entry. Thus, IFITM3 disrupts intracellular cholesterol homeostasis to block viral entry, further underscoring the importance of cholesterol in virus infection.

INTRODUCTION

Cellular lipid membranes form barriers that tightly regulate the entry and egress of many viruses. Cholesterol is essential in lipid raft membranes, organized sections within plasma membranes, endosomal compartments, and other organelles. Numerous studies have demonstrated that not only do lipid raft membranes and cholesterol play vital roles in cellular pathways and cell biological phenomena, but they also have critical functions in viral infection (Mañes et al., 2003; Schroeder, 2010). Specifically, membrane lipid rafts are involved in entry, assembly, and budding of many nonenveloped and enveloped viruses, such as influenza A virus (IAV), vesicular stomatitis virus (VSV), human immunodeficiency virus-1 (HIV-1), Epstein-Barr virus (EBV), Ebola virus, Marburg virus, and herpes simplex virus (HSV) (Chang et al., 2012; Gianni and Campadelli-Fiume, 2012; Veit and Thaa, 2011; Wang et al., 2009). Intracellular cholesterol levels increase by endocytosis of extracellular cholesterol as well as de novo biosynthesis (Ikonen, 2008; Ioannou, 2001). The modulation of intracellular cholesterol homeostasis within cells, especially in the endosomal compartment, has dramatic effects on the entry stage of viral infection (Carette et al., 2011; Danthi and Chow, 2004; Gruenberg, 2009; Kobayashi et al., 1999; Poh et al., 2012). Changes in intracellular cholesterol homeostasis during the course of an infection are therefore either part of a cellular reprogramming process facilitating viral replication and/or a specific infection-induced host defense response. Thus, intracellular cholesterol homeostasis may be a potential target for disrupting "virus-containing cargos" and reveal avenues to combat viral infections.

Under normal physiological conditions, cholesterol is delivered to endosomal compartments, subjected to hydrolysis, and then transported to the cytosol. In addition, de novo synthesized cholesterol, another source of cholesterol in the cell, must be transported from the endoplasmic reticulum (ER) to other organelles, such as endosomes, lysosomes, Golgi, mitochondria, and plasma membranes (Holthuis and Levine, 2005). Vesicle-associated membrane protein (VAMP)-associated protein A (VAPA) and oxysterol-binding protein (OSBP) are two important proteins implicated in these processes (Raychaudhuri and Prinz, 2010). Specifically, the major sperm protein (MSP) domain of VAPA interacts with the FFAT motif of OSBP to transfer cholesterol from the ER to organelles; however, detailed mechanisms of VAPA-OSBP complex-mediated cholesterol transport are still elusive (Holthuis and Levine, 2005; Levine, 2004). On the other hand, as seen in Niemann-Pick type C1 (NPC1) disease, disturbance in cholesterol transport from endosomal compartment to cytosol results in cholesterol accumulation in late endosomes and multivesicular bodies (MVBs) (Maxfield and Tabas, 2005; Subramanian and Balch, 2008). Because many viruses, including IAV and VSV, enter the cytoplasm by crossing the endosomal compartment with MVBs

(Uchil and Mothes, 2005), cholesterol accumulation in late endosomes and MVBs impairs viral function, preventing delivery of the viral capsid or genome to the cytosol (Chevallier et al., 2008; Sobo et al., 2007). For example, during VSV infection, fusion of the viral envelope with endosomal membranes and nucleocapsid release occur sequentially at two successive steps of the endocytic pathway; initial fusion occurs in transport intermediates between early and late endosomes, followed by the back-fusion of internal vesicles with the limiting membrane of late endosomes. The second step depends on the late endosomal phospholipid, lipid lysobisphosphatidic acid (LBPA), and is regulated by phosphatidylinositol-3-phosphate (PtdIns3P) signaling via the PtdIns3P-binding protein Snx16 (Kobayashi et al., 1999; Le Blanc et al., 2005). On the other hand, HIV-1 relies on cholesterol-laden lipid raft membrane microdomains for entry into and egress out of susceptible cells. Specifically, intact intracellular cholesterol trafficking pathways mediated by cholesterol-shuttling NPC1 are needed for efficient HIV-1 release and production (Tang et al., 2009). Furthermore, recent studies have also identified that membrane fusion mediated by filovirus glycoproteins and viral escape from the vesicular compartment require the NPC1 protein (Carette et al., 2011; Côté et al., 2011). Thus, integrity of membrane lipid rafts and cholesterol homeostasis are essential for the ordered assembly and release of a number of different infectious virus particles.

Host innate immunity is activated upon viral entry, thus acting as the first line of defense against viral infection, mainly via antiviral interferon (IFN)-stimulated genes (*ISGs*) (Sadler and Williams, 2008). Approximately, 300 *ISG* genes have been identified, but the exact molecular mechanisms of many remain elusive (Schoggins et al., 2011; Yan and Chen, 2012). We have recently shown that IFN-inducible transmembrane (IFITM) proteins restrict the replication of multiple viruses, including IAV, SARS coronavirus, filoviruses (Ebola and Marburg viruses), flaviviruses (dengue and West Nile viruses), and VSV (Bailey et al., 2012; Brass et al., 2009). Others have also demonstrated that IFITM proteins restrict HIV-1 (Lu et al., 2011). In contrast, IFITMs do not inhibit the entry processes of amphotropic mouse leukemia virus (MLV), Machupo virus (MACH), Lassa virus (LASA), or lymphocytic choriomeningitis virus (LCMV) (Diamond and Farzan, 2013). The IFITM isoforms are relatively small (~130 amino acids) and share a common topology of two conserved transmembrane domains, a short highly conserved cytoplasmic region, and luminal amino- and carboxyl termini (Siegrist et al., 2011; Wee et al., 2012). Recent studies showed that S-palmitoylation and ubiquitination of IFITM3 play crucial roles in its function (Yount et al., 2010, 2012) and that IFITM3 may influence v-ATPase complex activity and facilitates the subcellular localization of clathrin (Wee et al., 2012). Three additional studies showed that the N-terminal 21 amino acid residues of IFITM3 are required for its antiviral activity against VSV and IAV (Everitt et al., 2012; Jia et al., 2012; Weidner et al., 2010). Finally, IFITM-mediated restriction can be bypassed by inducing viral fusion at the plasma membrane, suggesting that the site or mechanism of viral entry can affect sensitivity to IFITM-mediated restriction (Huang et al., 2011). Despite current active investigation, a detailed mechanism of IFITM-mediated antiviral activity is still elusive.

In this study, we describe a mechanism by which IFITM proteins exert their antiviral activity. We found that IFITM1, IFITM2, and IFITM3 interact with VAPA, and this interaction antagonizes VAPA-OSBP function, disturbing intracellular cholesterol homeostasis, resulting in cholesterol-laden late endosomal compartments that block viral release to the cytosol. In contrast, VAPA expression facilitated the fusion of internal vesicles with the limiting membrane of endosomes, allowing viral release to the cytosol. IFITM inhibition of VAPA-OSBP functions to disturb the integrity of cholesterol homeostasis, and therefore blocking viral entry represents an antiviral strategy that offers itself as a target for therapeutic avenues to combat viral infections.

RESULTS

IFITM and VAPA Interaction

To identify how IFITM3 mediates antiviral activity, a yeast two-hybrid (Y2H) screening assay was performed. Full-length *IFITM3* was cloned into the pGBKT7 vector as bait, and AH109 yeast expressing IFITM3 was transformed with a human leukocyte matchmaker complementary DNA (cDNA) library. This Y2H screening revealed that IFITM3 interacts with full-length VAPA. An immunoprecipitation (IP) assay confirmed the interaction of IFITM1, IFITM2, and IFITM3 with endogenous VAPA in A549 cells (Figure 1A). Interaction of IFITM3 with VAPA was further confirmed under overexpression conditions (Figures 1B and 1C). To identify which domain(s) of VAPA are responsible for IFITM interaction, *VAPA* and *IFITM* were fragmented and cloned into the GAL4 activation and DNA binding vectors, respectively. Y2H mapping study revealed that the IFITM$^{108-128}$ fragment containing the transmembrane 2 (TM2) domain alone and the VAPA$^{169-248}$ fragment containing the coiled-coil domain (CCD) and transmembrane (TM) domain are responsible for their interaction (Figures 1D and 1E; Figure S1A available online). A pull-down assay with mammalian glutathione S-transferase (GST)-IFITM fusions further confirmed that the TM2 region of IFITM3 is sufficient for VAPA binding (Figures S1B and S1C). IFITM1 and IFITM3 showed similar binding affinity to VAPA, and both appeared to have a slightly higher binding affinity to VAPA than to VAPB (Figures S1D and S1E). These results demonstrate a specific interaction between IFITM and VAPA.

The interaction between VAPA and OSBP plays an important role in transferring cholesterol between ER and organelles for cholesterol homeostasis (Holthuis and Levine, 2005; Levine, 2004; Maxfield and Tabas, 2005). To test whether IFITM3 or OSBP affects the interaction between VAPA and OSBP or between VAPA and IFITM3, respectively, bacterially purified GST-VAPA fusion protein (Figure S1F) was mixed with whole-cell lysates containing OSBP and IFITM3, followed by GST pull-down (GST-PD) and immunoblotting assay. These experiments revealed that increasing VAPA-IFITM3 interaction led to decreasing VAPA-OSBP interaction, whereas increments of the OSBP did not affect VAPA-IFITM3 interaction (Figure 1F). These data indicate that IFITM3 blocks the interaction between VAPA and OSBP in a VAPA-binding dependent manner.

IFITM3-Mediated Restriction of Viral Infection Is Dependent on VAPA Expression

It was previously shown that the IFITM3 inhibits the early stage of viral entry (Brass et al., 2009; Feeley et al., 2011). To assess the effects of IFITM3-VAPA interaction on viral infection, human

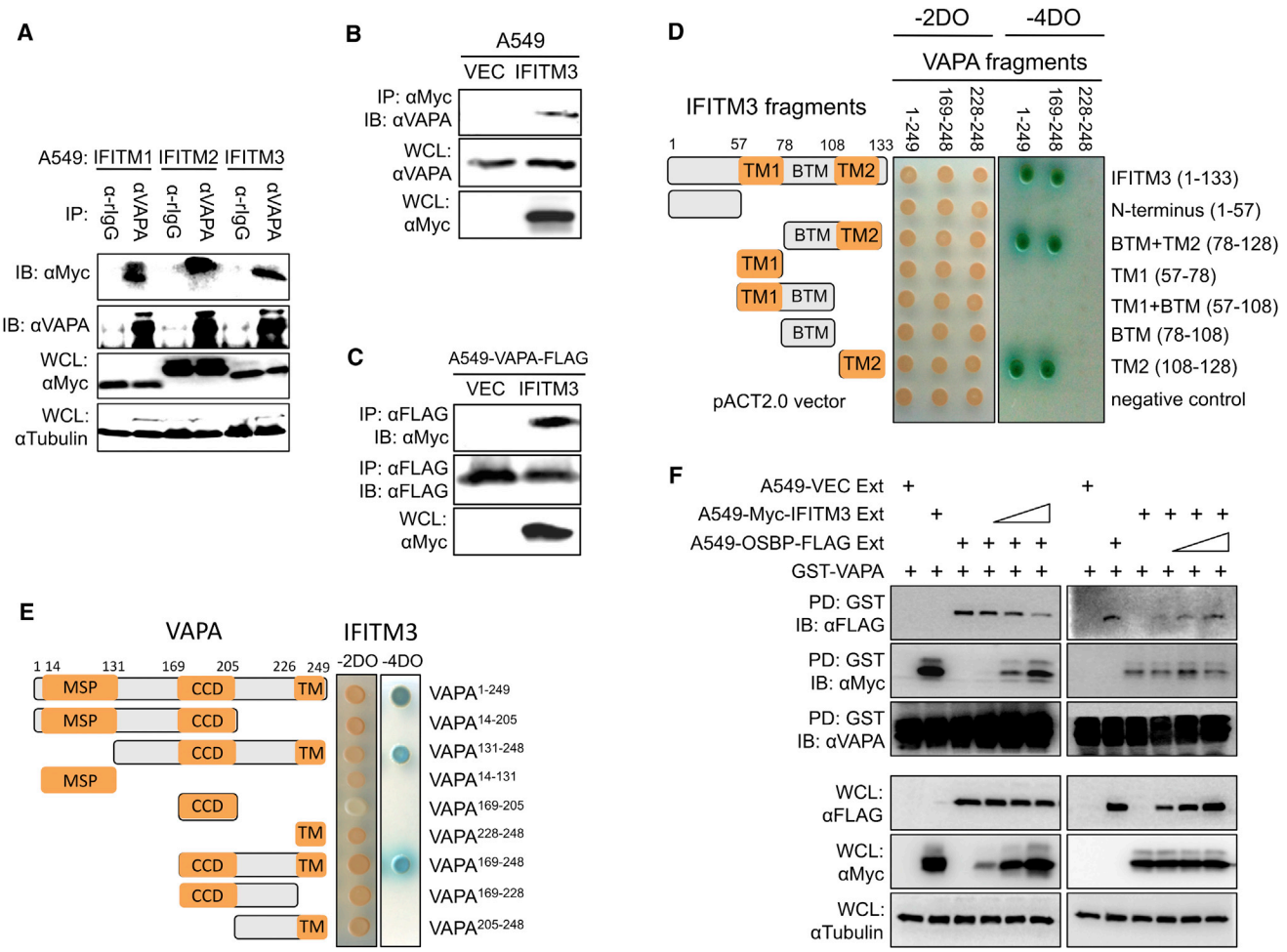

Figure 1. IFITMs Specifically Interact with VAPA, and IFITM3 Interaction Suppresses the Interaction between VAPA and OSBP

(A) Lysates of A549-IFITM1, A549-IFITM2, or A549-IFITM3 cells were used for immunoprecipitation (IP) with anti-VAPA antibody, followed by immunoblotting (IB) with anti-Myc antibody.

(B) Lysates of A549-Vector and A549-IFITM3 cells were used for IP and IB with the indicated antibodies. Whole-cell lysates (WCLs) were used for IB with the indicated antibodies.

(C) Lysates of A549-Vector-VAPA-FLAG and A549-IFITM3-VAPA-FLAG cells were used for IP and IB with the indicated antibodies.

(D) Various fragments of the *IFITM3* gene and three fragments of *VAPA* gene were used for Y2H assay.

(E) Various fragments of the *VAPA* gene and a full-length *IFITM3* gene were used for Y2H assay.

(F) Bacterially purified GST-VAPA protein was mixed with OSBP-containing cell lysates with increasing amounts of IFITM3-containing cell lysates (left panel), or bacterially purified GST-VAPA protein was mixed with IFITM3-containing cell lysates with increasing amounts of OSBP-containing cell lysates (right panel). Mixtures were incubated for 2 hr at 4°C, followed by GST pull-down (PD) and IB with the indicated antibodies. WCLs were used for IB with the indicated antibodies. See also Figure S1.

lung epithelial A549 cells expressing vector, IFITM3, VAPA, or IFITM3-VAPA (Figure S1G) were infected with VSV or IAV PR8 strain, and viral replication was then measured using a standard plaque assay. Not surprisingly, replication of both VSV and IAV was dramatically restricted in A549-IFITM3 cells but slightly elevated in A549-VAPA cells compared to A549-vector cells (Figures 2A, 2B, and 2C). VAPA expression in A549-IFITM3 cells effectively counteracted the IFITM3-mediated restriction of VSV and IAV replication (Figures 2A, 2B, 2C, and S1H). To further confirm the effect of VAPA expression on IFITM3 activity, endogenous VAPA expression in A549-vector and A549-IFITM3 cells was depleted by *VAPA*-specific short hairpin RNA (shRNA) (Figure S1I). Viral replication showed that although depletion of the *VAPA* gene expression apparently reduced VSV and IAV replication in A549-vector cells, this effect was more apparent in A549-IFITM3 cells (Figures 2D and 2E).

A single cycle of viral entry was also evaluated using defective pseudoretroviruses carrying various viral envelopes. As previously shown (Brass et al., 2009), IFITM3 effectively inhibited the entry of VSV, IAV PR8 (H1N1), and IAV Udorn (H3N1), but not lymphocytic choriomeningitis virus (LCMV), Moloney leukemia virus (MLV), Machupo virus (MACH), and Lassa virus (LASA) (Figures 2F and 2G). VAPA expression counteracted IFITM3-mediated antiviral activity, resulting in detectable increases of VSV and IAV entry, whereas VAPA depletion considerably suppressed VSV and IAV entry in mock-transfected as well as in IFITM3-expressing

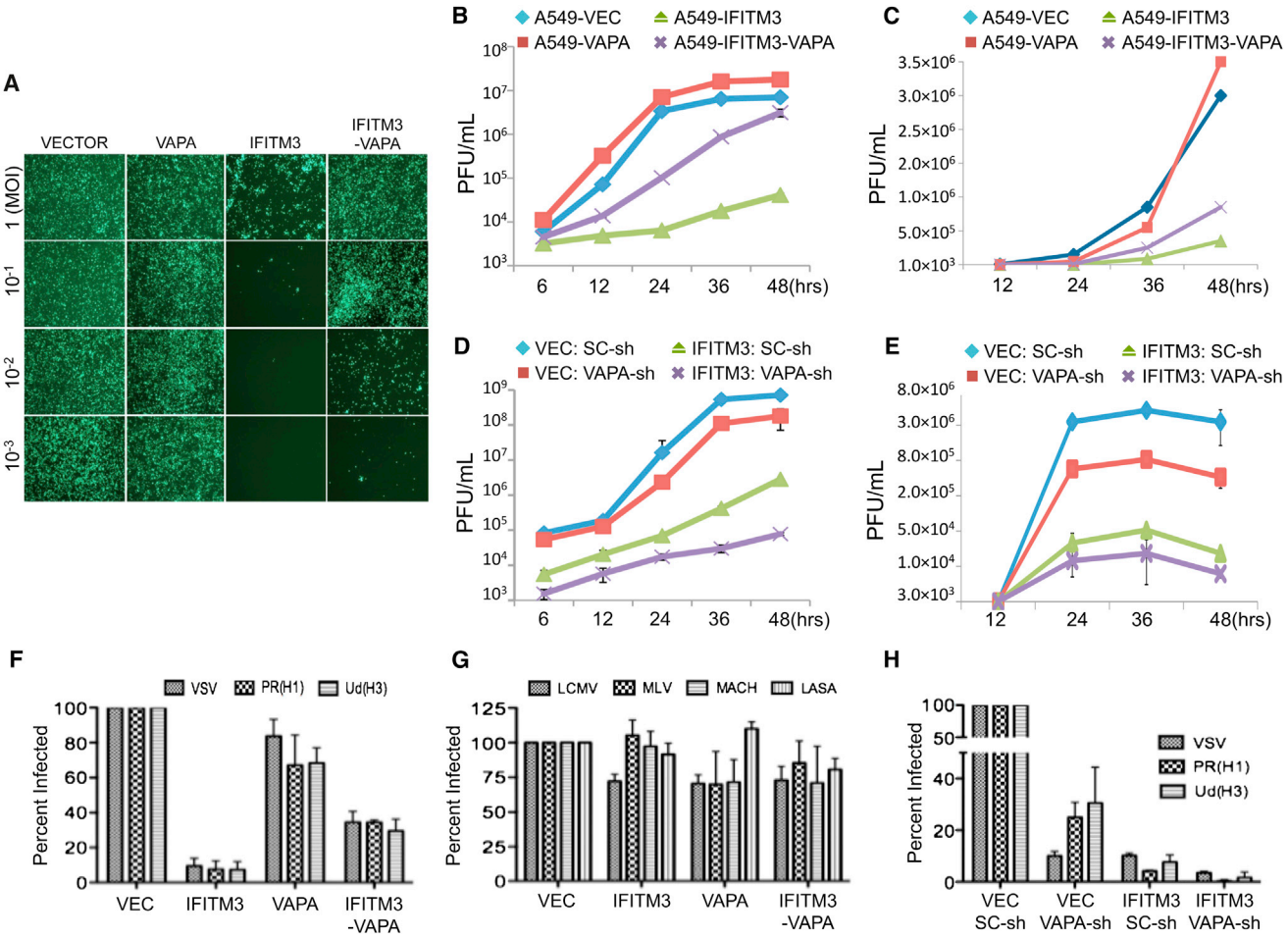

Figure 2. VAPA Antagonizes IFITM3-Mediated Inhibition of Viral Entry

(A) A549 cells were infected with various multiplicity of infection (m.o.i) of GFP-VSV, and replication levels were monitored by immunofluorescence microscopy (magnification: 4×).

(B) A549 cells were infected with VSV (m.o.i = 0.1), and VSV replications were determined by a standard plague assay. Values represent mean ± SD, n = 3 independent experiments.

(C) A549 cells were infected with the IAV PR8/H1N1 strain (m.o.i = 0.1), and IAV replications were determined by a standard plague assay. Values represent mean ± SD, n = 3 independent experiments.

(D) A549-Vector and A549-IFITM3 cells were infected with lentivirus carrying either VAPA-shRNA (VAPA-sh) or SC-shRNA (SC-sh). After 2 days, A549 cells were infected with the VSV PR8/H1N1 strain (m.o.i = 0.1), and VSV replications were determined by a standard plague assay. Values represent mean ± SD, n = 3 independent experiments.

(E) A549-Vector and A549-IFITM3 cells were infected with lentivirus carrying either VAPA-shRNA (VAPA-sh) or SC-shRNA (SC-sh). After 2 days, A549 cells were infected with the IAV PR8/H1N1 strain (m.o.i = 0.1), and IAV replications were determined by a standard plague assay. Values represent mean ± SD, n = 3 independent experiments.

(F and G) A549 cells were incubated with MLV-EGFP virus pseudotyped with the indicated envelope protein (VSV, IAV H1N1 [PR8], IAV H3N1 [Udorn], LCMV, MLV, MACH, or LASA). Viral entry is expressed as mean EGFP fluorescence relative to vector control cells, as measured by flow cytometry. Values represent mean ± SD, n ≥ 3 independent experiments.

(H) A549-Vector and A549-IFITM3 cell lines were infected with lentivirus carrying either VAPA-shRNA (VAPA-sh) or SC-shRNA (SC-sh). After 2 days, cells were incubated with defective MLV-EGFP pseudotyped with the envelope protein of VSV, IAV H1N1 (PR8), or IAV H3N1 (Udorn). Viral entry is expressed as mean EGFP fluorescence relative to vector control cells, as measured by flow cytometry. Values represent mean ± SD, n ≥ 3 independent experiments. See also Figure S2.

cells (Figures 2F, 2G, and 2H). However, neither expression nor depletion of the *OSBP* gene showed any detectable effects on VSV entry and replication (Figures S2A, S2B, and S2C; data not shown). These results collectively demonstrate that IFITM3-mediated restriction of viral infection is dependent on VAPA expression, suggesting that the *VAPA* gene plays an important role in viral entry by antagonizing IFITM3 activity.

IFITM3 Expression Causes Cholesterol-Laden Endosomal Compartments

IFITM3 can be detected at the plasma membrane (Figure S2D) but is localized primarily in endosomal and lysosomal compartments as indicated by colocalization endosomal and lysosomal markers LAMP1 and CD63 (Figure S2E). Furthermore, IFITM3 mostly colocalized with Rab7, though weakly with Rab5,

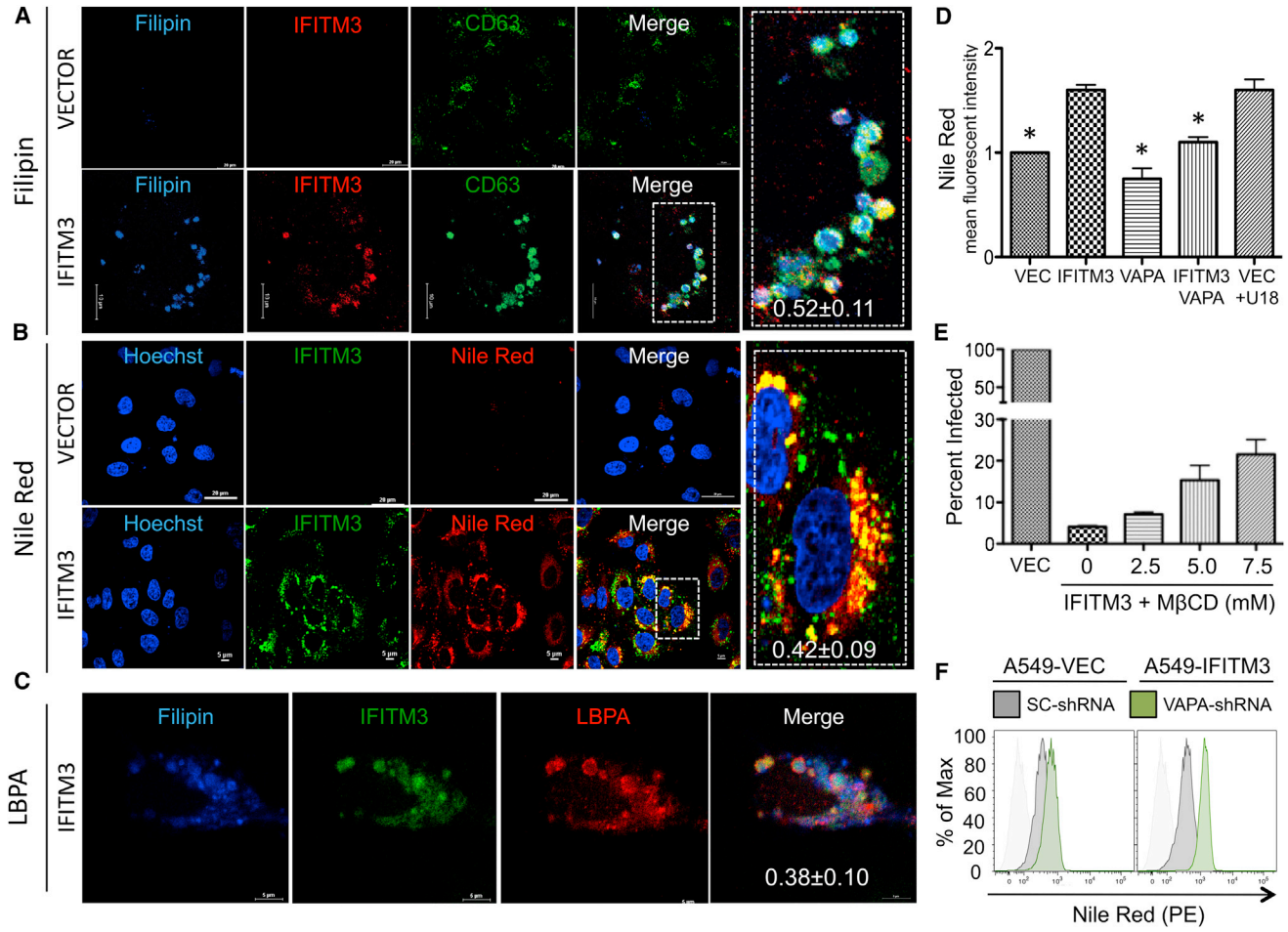

Figure 3. IFITM3 Induces Cholesterol-Laden Endosomal Compartments

(A and B) A549-Vector or A549-IFITM3 cells were stained with filipin (A) or Nile Red (B), together with anti-Myc (IFITM3) or anti-CD63 antibody. Scale bars, 10 and 20 μm. The inserts at the right panels show the magnified images. The metric values (mean ± SD) in the inserts represent colocalization quantification of either filipin with IFITM3 (0.52 ± 0.11) or Nile Red with IFITM3 (0.42 ± 0.09) calculated by Pearson's correlation coefficient based on ≥20 cells.

(C) A549-IFITM3 cells were stained with filipin, together with anti-Myc (IFITM3) and anti-LBPA antibody. Scale bar, 5 μm. Colocalization between LBPA and IFITM3 was quantified as 0.38 ± 0.10 (Pearson's coefficient, mean ± SD, n ≥ 20).

(D) A549-Vector, A549-IFITM3, A549-VAPA, and A549-IFITM3-VAPA cells were stained with Nile Red dye to measure their intracellular cholesterol levels by flow cytometry. The mean fluorescence intensities (MFI) were compared and presented as relative folds compared with those of A549-Vector cells. As a positive control, A549-Vector cells were treated with 2 μg/ml U18666A (U18), a cholesterol transport inhibitor, to induce cholesterol accumulation in endosomal compartments. Values represent mean ± SD, n > 3 independent experiments. Significant differences (p value < 0.05), compared to IFITM3, are marked by an asterisk.

(E) A549-IFITM3 cells were washed 3–5 times with PBS and then treated with different concentrations (mM) of MβCD in free-serum media at 37°C for 45 min. Cells were then washed three times and incubated with defective MLV-EGFP pseudotyped with VSVgp. Viral entry is expressed as mean EGFP fluorescence relative to A549-Vector cells, as measured by flow cytometry. Values represent mean ± SD, n ≥ 3 independent experiments.

(F) A549-Vector and A549-IFITM3 were infected with lentivirus carrying VAPA-shRNA or SC-shRNA. After two days, cells then fixed, stained with Nile Red, and subjected to flow cytometry analysis to measure intracellular cholesterol levels. See also Figure S3.

indicating the late endosomal localization of IFITM3 (Figure S2F). Additionally, we excluded other cellular compartments, such as lipid droplet-containing vacuoles, as sites of IFITM3 localization (Figure S3A). Confocal microscopy revealed that endogenous VAPA partially colocalized with IFITM3 in the enlarged CD63-containing endosomal compartments of A549-IFITM3 cells (Figure S3B). These data demonstrate that IFITM3 is mainly present in late endosomal compartments, where it partly colocalizes with VAPA. Although IFITM3 expression dramatically affects the biogenesis of endosomal compartments, leading to morphological changes of endosomal compartments (Feeley et al., 2011), its expression did not affect endosomal CD63 and LAMP1 protein levels (Figure S3C). Because IFITM proteins block the interaction between VAPA and OSBP that mediates transfer of cholesterol between ER and organelles (Ikonen, 2008), we determined the intracellular cholesterol levels using the histochemical cholesterol markers, filipin and Nile Red dyes. The CD63-positive endosomal compartments of A549-IFITM3 cells showed much higher cholesterol levels than those of A549-vector cells (Figures 3A and 3B; Figures S3A, top panel, and S3D), and these cholesterol-laden IFITM3-positive endosomal compartments were also

enriched with lysobisphosphatidic acid (LBPA), a phospholipid that has an important role in cholesterol homeostasis (Chevallier et al., 2008; Kobayashi et al., 1999) (Figure 3C). Flow cytometry and biochemical analyses showed that intracellular cholesterol levels (total cholesterol and free cholesterol) were considerably increased upon IFITM3 expression, whereas they were apparently decreased by VAPA expression (Figures 3D and S3E). Furthermore, IFITM1 or IFITM2 expression led to the increased endosomal cholesterol levels as seen with IFITM3 expression (Figures S4A and S4B). Because cholesterol-laden endosomal compartments suppress viral release from late endosomes to the cytosol by inhibiting the fusion process (Chevallier et al., 2008; Le Blanc et al., 2005), IFITM3-expressing cells were treated with the cholesterol-depleting agent methyl-β-cyclodextrin (MβCD), followed by Nile Red dye staining to detect intracellular cholesterol levels or infection with defective pseudoretroviruses to measure VSV entry. MβCD treatment of IFITM3-expressing cells detectably reduced endosomal cholesterol levels and increased single-cycle viral entry (Figures 3E and S4C). Furthermore, shRNA-mediated depletion of VAPA expression also increased endosomal cholesterol levels (Figures 3F, S4D, and S4E), which correlates with decreases in viral entry and replication (Figures 2D, 2E, and 2H). These findings collectively indicate that IFITM3-mediated disturbance of the VAPA-OSBP interaction results in cholesterol accumulation in endosomal compartments, which ultimately inhibits viral entry.

IFITM3-VAPA Interaction Is Required for the Accumulation of Endosomal Cholesterol and the Inhibition of Viral Entry

To demonstrate the specificity of IFITM3 action, the IFITM3$^{\Delta TM2}$ mutant that lacked its C-terminal TM2 region and was incapable of interacting with VAPA (Figure S4F) was tested for its ability to disturb cholesterol homeostasis and viral entry. Because of the loss of VAPA interaction, expression of the IFITM3$^{\Delta TM2}$ mutant neither led to the accumulation of endosomal cholesterol nor blocked GFP-IAV and GFP-VSV replication (Figures S4G and S4H). A549-IFITM3$^{\Delta TM2}$ cells were also incapable of inhibiting viral entry when challenged in a single-cycle infection with defective pseudoretroviruses carrying VSV, IAV PR8 (H1N1), and IAV Udorn (H3N1) glycoprotein (Figure S4I). However, the IFITM3$^{\Delta TM2}$ mutant was apparently expressed at a lower level compared to the IFITM3 wild-type (WT) and present throughout the cytoplasm, unlike IFITM3 WT (Figures S4F and S4G). For this reason, the TM2 region of IFITM3 was thus replaced with the transmembrane region of CD4 or of transferrin receptor 1 (TR) to generate the IFITM3-CD4 and IFITM3-TR chimeras, respectively (Figure 4A). Whereas both mutant chimeras colocalized with CD63 similar to IFITM3 WT, neither the IFITM3-CD4 nor the IFITM3-TR chimera was capable of binding VAPA (Figures 4B and 4C) and had any detectable effect on the interaction between VAPA and OSBP (Figure S4J). Consequently, their expression displayed little or no effect on the accumulation of endosomal cholesterol (Figures 4B and S3E) and on the replication of GFP-IVA and GFP-VSV (Figure 4D). Finally, the IFITM3-CD4 and IFITM3-TR chimeras were also incapable of inhibiting viral entry when challenged in a single-cycle infection with defective pseudoretroviruses carrying VSV, IAV PR8 (H1N1), and IVA Udorn (H3N1) glycoprotein (Figure 4E). These results collectively indicate that the IFITM3 and VAPA interaction triggers the accumulation of endosomal cholesterol and thereby inhibits viral entry.

IFITM3 Induces MVB Formation and VAPA Triggers the Fusion between the Intraluminal Vesicles and Limiting Membrane of MVBs

Confocal microscopy showed that IFITM3 expression led to a pronounced enlargement of CD63-containing compartments, which costained with the filipin cholesterol marker (Figure 5A, upper panel). Consistently, transmission electron microscopy (TEM) and immunogold electron microcopy (EM) also revealed that IFITM3 robustly induced multivesicular body (MVB) formation and was primarily present in the abundant intraluminal vesicles, whereas a minor population of IFITM3 was also present on the cell surface (Figures 5B and S5A). Strikingly, confocal microscopy showed that VAPA expression altered these IFITM3-induced enlarged MVBs to become "ring"-shaped structures that hardly costained with filipin (Figure 5A, lower panel). TEM and immunogold EM also revealed that upon VAPA expression in A549-IFITM3 cells, the intraluminal vesicles of MVBs were pushed to the edges and apparently fused with the surrounding limiting membrane (Figures 5C and S5B) and that levels of this "ring form" structure of the endosomal compartments of A549-IFITM3-VAPA cells were markedly higher than those of A549-IFITM3 cells (Figure 5D). Of note, immunogold EM also showed that VAPA was present in the cytoplasmic ER and endosomal compartments of the IFITM3 and IFITM3-VAPA cell lines (Figures S5C and S5D). A549-vector and A549-VAPA cells showed normal structural morphology though A549-VAPA cells exhibited swollen endoplasmic reticulum. There were no alterations in MVB formation in both cell lines (Figures S5E and S5F). These results demonstrate that IFITM3 expression robustly induces MVB formation, whereas VAPA expression appears to trigger the fusion between the intraluminal vesicles and limiting membrane of MVBs.

IFITM3 Impedes Vesicle Membrane Fusion to Block the Cytosolic Release of Virion Particles

It has been shown that during VSV entry, viral fusion occurs in the abundant internal vesicles of MVBs first, followed by the back-fusion of these internal vesicles with the limiting MVB membrane, ultimately leading to the cytoplasmic delivery of VSV nucleocapsids (Le Blanc et al., 2005; Uchil and Mothes, 2005). As shown in Figure 2, IFITM3 inhibits the early stage of VSV entry, but this inhibition was compromised by VAPA expression. Consistently, TEM also revealed that VSV particles were extensively packed within the MVBs of A549-IFITM3 cells (Figures 6A and Figure S6A). On the other hand, only limited numbers of VSV particles were observed in the MVBs of A549-IFITM3-VAPA cells, where the intraluminal vesicles of MVBs were apparently fused with the surrounding limiting membrane (Figures 6B and S6B). To further delineate VSV entry, A549-IFITM3 and A549-IFITM3-VAPA cells were immunolabeled with 15 nm nano-gold-conjugated anti-Myc antibody to detect Myc-tagged IFITM3 and 30 nm nano-gold-conjugated anti-VSV-G antibody to detect the VSV glycoprotein. Immunogold EM revealed that the VSV-G protein accumulated in the abundant intraluminal vesicles of MVBs of A549-IFITM3 cells, where IFITM3 was also present

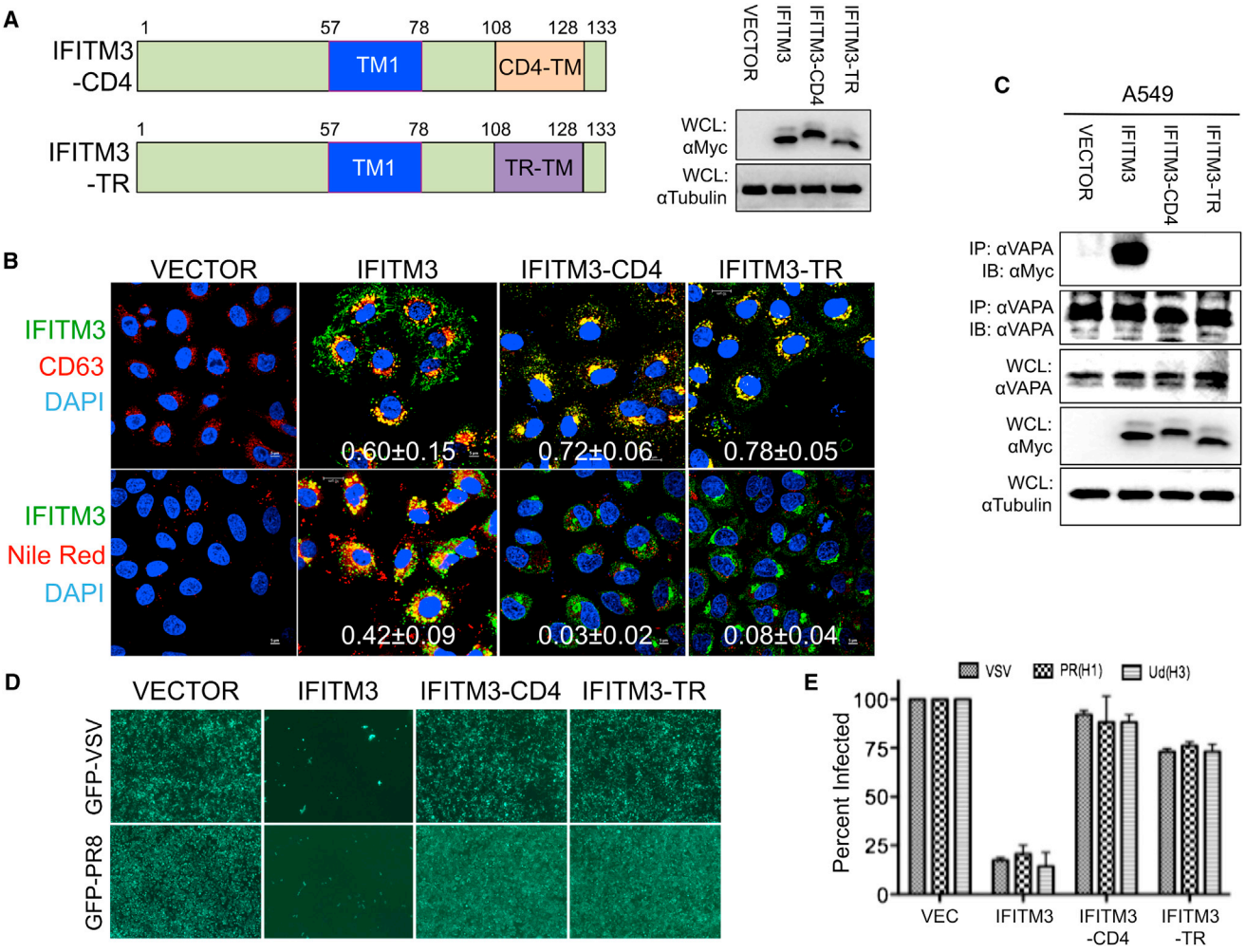

Figure 4. IFITM3-VAPA Interaction Is Required to Restrict Viral Entry

(A) Schematic illustration of IFITM3 chimera carrying the CD4 transmembrane (IFITM-CD4) or transferrin receptor transmembrane (IFITM3-TR). WCLs were used for IB with the indicated antibodies.

(B) A549-Vector, A549-IFITM3, A549-IFITM3-CD4, and A549-IFITM3-TR cells were fixed and stained with anti-Myc (IFITM3), anti-CD63, or Nile Red dye for confocal microscopy. DAPI was used to stain the nucleus. Scale bar, 5 μm. The metric values (mean ± SD) represent the quantitative assessment of the colocalization of CD63 (top panel) and Nile Red (bottom panel) with IFITM3 WT and chimeras (Pearson's coefficient, mean ± SD, $n \geq 20$).

(C) Lysates of A549-Vector, A549-IFITM3, A549-IFITM3-CD4, and A549-IFITM3-TR cells were used for IP and IB. WCLs were used for IB analysis to show expressions of VAPA, IFITMs, and tubulin.

(D) A549-Vector, A549-IFITM3, A549-IFITM3-CD4, and A549-IFITM3-TR cells were infected with GFP-VSV (top panel) or GFP-IAV PR8 (bottom panel). At 48 hr postinfection, cells were photographed under immunofluorescence microscopy (magnification: 4×).

(E) A549-Vector, A549-IFITM3, A549-IFITM3-CD4, and A549-IFITM3-TR cells were infected with defective MLV-EGFP pseudotyped with the envelope proteins of VSV, IAV H1N1 (PR8), or IAV H3N1 (Udorn). Viral entry is expressed as mean EGFP fluorescence relative to vector control cells, as measured by flow cytometry. Values represent mean ± SD, $n \geq 3$ independent experiments. See also Figure S4.

(Figures 6A and S6C). In striking contrast, both the VSV glycoprotein and IFITM3 were located at the surrounding limiting membrane of MVBs in A549-IFITM3-VAPA cells (Figures 6B and S6D). These results demonstrate that VSV particles accumulate in the intraluminal vesicles of MVBs in IFITM3 expressing cells, whereas they are redistributed near to the surrounding limiting membrane of MVB upon VAPA expression. This suggests that IFITM3 compromises VAPA function to disturb endosomal cholesterol levels, blocking fusion between the intraluminal vesicles and limiting membrane of MVBs and thereby inhibiting viral release to the cytosol.

DISCUSSION

IFITM proteins are a family of small ISGs that possess various functions, including adhesion, antiproliferation, apoptosis, development, bone mineralization, and tumor progression (Siegrist et al., 2011; Zhang et al., 2012). Although IFITM proteins were identified around two decades ago, their antiviral role was discovered recently and has been suggested to be a potential target for antiviral therapy against human pathogenic viruses, including IAV, Ebola virus, dengue virus, West Nile virus, and SARS coronavirus. Despite active investigations, a detailed

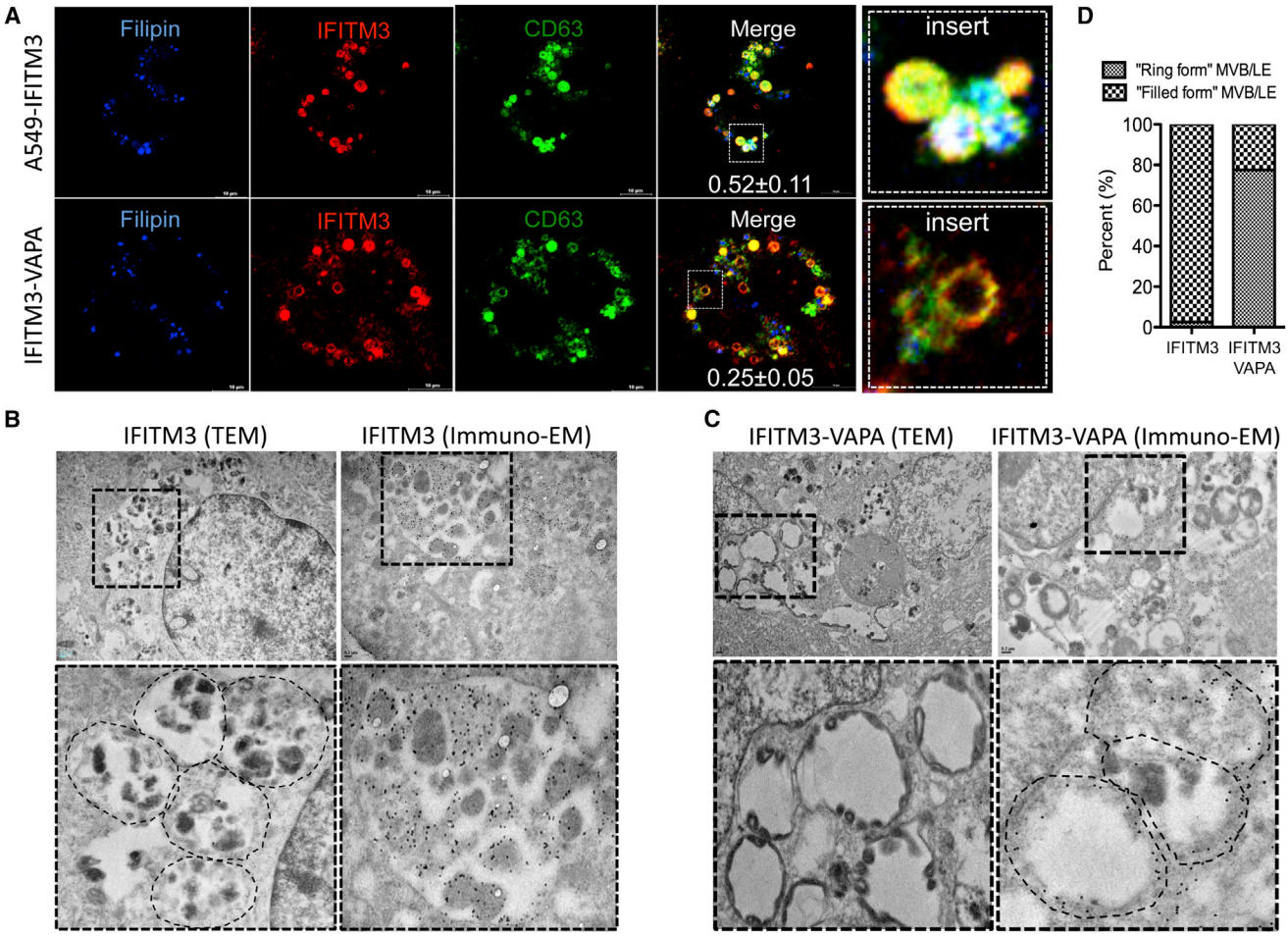

Figure 5. Effects of IFITM3 and VAPA Expression on MVB Structures

(A) A549-IFITM3 and A549-IFITM3-VAPA cells were stained with filipin, anti-Myc (IFITM3), and anti-CD63 for confocal microscopy. The inserts at the right panels show the magnified images of the "filled form" (top panel) or the "ring form" (bottom panel) of endosomal compartments. Scale bar, 10 μm. The numbers indicate the Pearson's correlation coefficient for colocalization of filipin and IFITM3 within endosomal compartments (mean ± SD, n ≥ 100 endosomal compartments).
(B and C) A549-IFITM3 and A549-IFITM3-VAPA cells were subjected to TEM and immunogold EM (anti-Myc and 15 nm gold particle-conjugated secondary antibody) as described in the Experimental Procedures. Magnified images of the inserts are shown in the bottom of the panel. Scale bar, 0.2 μm.
(D) Bar graphs represent the percentages of the "filled form" or the "ring form" structure of endosomal compartments within A549-IFITM3 and A549-IFITM3-VAPA cells from TEM images (n ≥ 100 endosomal compartments). See also Figure S5.

IFITM-mediated antiviral mechanism has been elusive. In this study, we report that IFITM1, IFITM2, and IFITM3 interact with VAPA, and this interaction antagonizes VAPA-OSBP function, disturbing intracellular cholesterol homeostasis, resulting in cholesterol-laden MVBs and late endosomes and thereby blocking viral release to the cytosol (Figure 7).

VAPA and VAPB are type II membrane proteins that are conserved from yeast to human and generally localize in the ER and other subcellular organelles (Lev et al., 2008). VAPA is involved in vesicle transport and membrane fusion though the precise details of its functions are unclear. It also plays an important role in cholesterol homeostasis through its interaction with cytosolic cholesterol sensor, OSBP (Holthuis and Levine, 2005; Maxfield and Tabas, 2005; Raychaudhuri and Prinz, 2010). VAPA is composed of three domains: a major sperm protein (MSP) domain, a coiled-coil domain (CCD), and a transmembrane (TM) domain. Based on a previous report (Wyles et al., 2002) and our study, the N-terminal MSP domain of VAPA sufficiently binds to OSBP, whereas the central CCD and C-terminal TM of VAPA are responsible for IFITM interaction. These suggest that VAPA may independently interact with OSBP and IFITMs, yet we found that IFITM3 interaction effectively suppressed the interaction between VAPA and OSBP. On the other hand, neither OSBP expression nor OSBP depletion had effect on the IFITM3-VAPA interaction and IFITM3-mediated antiviral activity. However, these results may not be conclusive because there are at least 12 different isoforms of OSBP (Raychaudhuri and Prinz, 2010). Nevertheless, our result suggests that IFITM3 interaction may considerably change VAPA structure or localization to disrupt OSBP binding and thus disturb intracellular cholesterol homeostasis. Two reports have recently shown that S-palmitoylation of the membrane-proximal cysteine residue of IFITM3 positively impacts its antiviral activity (Yount et al., 2010), whereas the posttranslational K48 and K63 ubiquitination of IFITM3 have

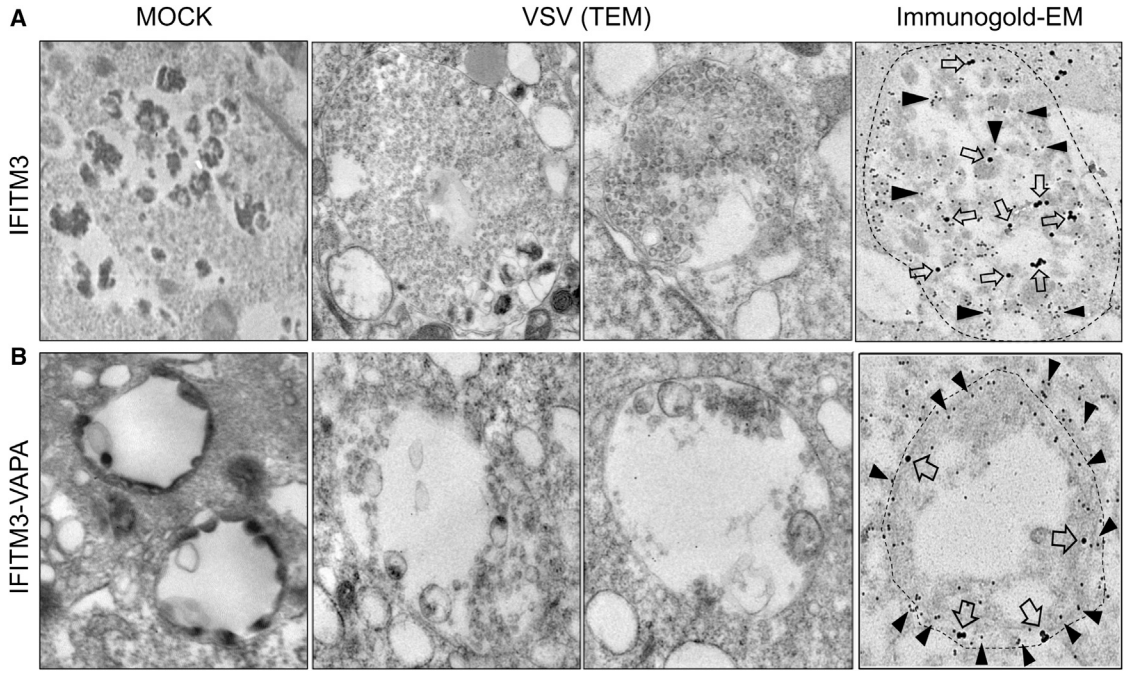

Figure 6. TEM and Immunogold EM of VSV-Infected A549-IFITM3 and A549-IFITM3-VAPA Cells

(A and B) A549-IFITM3 and A549-IFITM3-VAPA were mock infected (left panel) or with high titers of VSV for 1 hr (rest of panels). Then cells were washed to remove unbound viruses and subjected to TEM (scale bar, 0.1 μm) and immunogold EM (scale bar, 0.2 μm) as described in the Experimental Procedures. Dual immunogold labeling was performed with anti-Myc antibody and 15 nm gold particle-conjugated secondary antibody (IFITM3, filled triangle) and anti-VSVgp antibody and 30 nm gold particle-conjugated secondary antibody (VSVgp, open arrow). The areas of particular MVBs are marked by dashed lines. See also Figure S6.

negative effect on its antiviral activity (Yount et al., 2012). Furthermore, based on posttranslational modification studies, a new dual-pass transmembrane topology of IFITM, in which the N terminus and C terminus of IFITM are concurrently cytoplasmic (Yount et al., 2012), has been introduced. Jia and colleagues (Jia et al., 2012) have also shown that the first 21 amino acids of the IFITM3 N terminus are important for IFITM3 relocation to the endosomal compartment and lacking of this region impairs IFITM3 function; specifically, the tyrosine residue at the PPNY motif (amino acids 17–20) is critical for IFITM3 function. Although we and others (Diamond and Farzan, 2013) showed that the IFITM termini existed extracellularly at the plasma membrane, this new anticipated IFITM topology would not be inconsistent with our proposed model (Figure 7) because the TM2 of IFITM3 interacts with VAPA to control intracellular cholesterol levels. It has been shown that the Norwalk virus nonstructural protein p48 interacts with VAPA, and this interaction affects intracellular trafficking pathways (Ettayebi and Hardy, 2003). In addition, hepatitis C virus (HCV) has been shown to target both VAPs and OSBP to regulate viral replication. Specifically, the NS5A and NS5B proteins of HCV interact with VAPA and VAPB isoforms, and these interactions positively affect HCV replication (Gao et al., 2004; Hamamoto et al., 2005). Additionally, the N-terminal domain of the HCV NS5A protein interacts with OSBP, which is important for HCV particle release (Amako et al., 2009). However, none of these studies have detailed how these interactions specifically affect viral replication and maturation. Because cholesterol is an essential molecule for the life cycle of HCV, targeting VAPA and OSBP may not only play a significant role in HCV replication and pathogenesis but may also lead to the evasion of IFITM-mediated antiviral activity. These studies are currently under active investigation.

Accumulation of cholesterol within late endosomal compartments has been shown to impair their function, significantly impairing the infection of certain viruses that enter the cell through endocytosis, such as IAV, VSV, and dengue virus (Lakadamyali et al., 2004; Pattanakitsakul et al., 2010). We showed that IFITM3 expression induces substantial accumulation of cholesterol within MVBs and late endosomal compartments in a VAPA-binding-dependent manner. We also reproducibly observed the transient increase of cholesterol accumulation in endosomes as well as the pronounced enlargement of cholesterol-enriched late endosomal compartments upon IFN-β treatment (data not shown), suggesting that our observations of IFITM3 expression are physiologically relevant. However, levels of the intracellular cholesterol accumulation induced by IFN-β treatment were weaker than those induced by IFITM3 overexpression, which may be because IFN-β treatment affects expressions of over 300 genes, including the genes for cholesterol synthesis and cholesterol efflux. Furthermore, a recent paper (Roth and Whittaker, 2011) has reported that the endosome-specific LBPA selectively increases the rate of VSV G-mediated membrane fusion, but not the rate of IAV HA-mediated membrane fusion. On the other hand, the HA-mediated membrane fusion is dependent on the dynamic molecular shape of lipids because it is inhibited by the inverted cone-shaped lipid lysophosphatidylcholine but promoted by oleic acid (Chernomordik et al., 1997). In contrast, we show that the increase of endosomal cholesterol

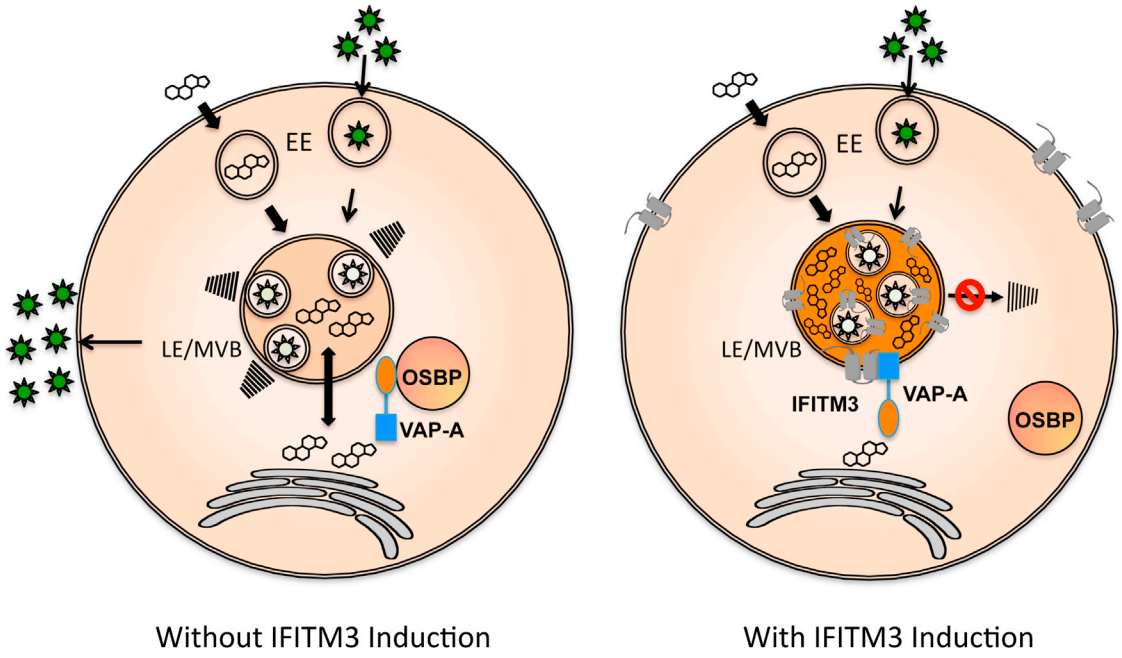

Figure 7. Schematic Model of IFITM3-Mediated Inhibition of Viral Entry

Schematic model represents viral infection in the absence (left panel) or presence (right panel) of IFITM induction. Virions (depicted as stars) enter the cell by endocytosis, are subsequently transferred to early endosome (EE), and are finally transferred to late endosome/multivesicular body (LE/MVB). In the absence of IFITM induction under normal cholesterol (depicted as its chemical shape) homeostasis conditions, the intraluminal virion-cargo-containing vesicles or virion particles finally fuse with the limiting membrane to release viral genome or nucleocapsid to the cytosol. In the presence of IFITM induction, IFITM-VAPA interaction disturbs intracellular cholesterol homeostasis, leading to the accumulation of cholesterol in LE/MVB. This consequently blocks the fusion of the intraluminal virion-cargo-containing vesicles or virion particles with the limiting membrane of LE/MVB compartments.

induced by IFITMs leads to the efficient inhibition of VSV and IAV entry, suggesting that each lipid moiety may have different selectivity and activity to regulate fusion events upon viral entry.

When the IFITM3 TM2 region was deleted or replaced with the TM regions of other proteins, VAPA interaction was completely lost, and accordingly, there was no cholesterol accumulation (Figure 4; Figures S4F–S4I). Interestingly, IFITM3-expressing cells show similar phenotypes to cells derived from NPC1 disease, an autosomal disorder with massive accumulation of cholesterol in late endosomal compartments (Peake and Vance, 2010; Subramanian and Balch, 2008). When NPC1 cells were challenged with various viruses, they also showed defect in viral infection, particularly at the entry step (Gruenberg, 2009; Kobayashi et al., 1999; Le Blanc et al., 2005). Furthermore, recent studies have identified that membrane fusion mediated by filovirus glycoproteins and viral escape from the vesicular compartment require the NPC1 protein. Specifically, NPC1 directly binds the viral glycoprotein (GP), which ultimately facilitates membrane fusion to induce viral release to the cytosol (Carette et al., 2011; Côté et al., 2011). Several pieces of evidence also indicate that members of the Rab GTPase family, such as Rab7 and Rab9, may impair cholesterol accumulation, and thus expression of these Rab GTPases complemented the defects seen in NPC1 cells, decreasing endosomal cholesterol levels and subsequently allowing viral infection (Ganley and Pfeffer, 2006; Lebrand et al., 2002; Narita et al., 2005; Zhang et al., 2009). However, expression of the *Rab7*, *NPC1*, or *NPC2* gene in A549-IFITM3 cells neither decreased endosomal cholesterol levels nor increased VSV and IAV infection (J.U.J. and S.A.-B.-O., unpublished data). In contrast, VAPA expression reduced endosomal cholesterol levels and ultimately enhanced VSV and IAV infection. Furthermore, the accumulation of cholesterol in late endosome of NPC cells and U18666A-treated cells led to a 2- to 3-fold increase in the size of the compartments. Most importantly, the properties and dynamics of the intraluminal vesicles of late endosomes showed reduced back fusion with the limiting membrane and blocked VSV release to the cytosol (Sobo et al., 2007). These suggest that the pathological accumulation of cholesterol induced by IFITM3 dramatically perturbs the fusion between the intraluminal vesicles or virion-containing compartments and the limiting membrane of MVBs, ultimately blocking viral release to the cytosol (Figure 7). These also indicate that IFITM3-expressing cells phenocopy NPC1 cells but utilize a different mechanism to induce the accumulation of endosomal cholesterol and thereby block viral entry. Of note, IAV and VSV use the classical endocytosis pathway that is dependent of caveolin- and clathrin-coated pits. After endocytosis, the virions ultimately travel to lysosomal compartments for cytosolic release, which is targeted by IFITM3. However, MLV is generally released to cytosol right after endocytosis without reaching lysosomal compartments. Specifically, upon fusion event between the MLV particles and host plasma membranes, virion cores are immediately delivered to the cytoplasm (Diamond and Farzan, 2013). Arenaviruses, including LCMV, LASA, and MACH, are internalized to cell via an unusual pathway of endocytosis that is independent of clathrin and caveolin (Kunz, 2009; Rojek

and Kunz, 2008). Thus, the IFITM3 action at the lysosomal compartments appears to be a key factor for its specific effect on IAV and VSV entry. In summary, our study shows an antiviral strategy in which IFITM proteins, as specific infection-induced host defense effectors, target VAPA to deregulate the integrity of cholesterol homeostasis necessary for the ordered release of infectious virion particles. These observations also offer IFITMs as targets for therapeutic avenues to combat viral infections.

EXPERIMENTAL PROCEDURES

Yeast Two-Hybrid Screening

IFITM3 full-length cDNA (NM_021034) was purchased from Open Biosystems (Lafayette, CO, USA) and cloned into the BamHI-*EcoRI* sites of the pGBKT7 vector (Clontech Laboratories, Mountain View, CA, USA) as bait. *Saccharomyces cerevisiae*, strain AH109, was transformed with the pGBKT7-IFITM3 vector. AH109 yeast expressing IFITM3 was subjected to Y2H library-scale transformation. A human leukocyte matchmaker cDNA library fused to a GAL4-activating domain in the pACT2 vector (Clontech Laboratories) was utilized for Y2H library-scale screening in accordance with Matchmaker Two-Hybrid System 3 instructions (Clontech Laboratories).

Transfection of IFITM3, VAPA, and OSBP

VAPA cDNA was purchased (Open Biosystems) and PCR cloned into the EcoRI-BamHI site of the lentivector pCDH-MCS-EF1-Neo mammalian expression system (System Biosciences, Mountain View, CA, USA). Puromycin-resistant A549-IFITM3 and A549-vector cells were infected by lentivirus pseudotyped with the Machupo virus glycoprotein (MACHgp) carrying VAPA or VAPA-FLAG. MACHgp was used instead of vesicular stomatitis virus glycoprotein (VSVgp) because IFITM3 robustly restricts VSVgp-mediated entry (Brass et al., 2009).

Cell Culture, Immunoblotting, Immunoprecipitation, and GST Pull-Down

A549 cells were maintained in RPMI-1640 medium supplemented with 10% fetal bovine serum (Gibco Life Technologies, Grand Island, NY, USA), nonessential amino acids (Gibco), and appropriate antibiotics. Puromycin (Invitrogen, Carlsbad, CA, USA) and G418 antibiotics were used to generate cell lines. Western blot (WB) and coimmunoprecipitation (coIP) were performed in accordance with standard protocols.

VAPA shRNA Silencing

To deplete *VAPA* gene expression, several shRNAs targeting the *VAPA* gene were designed and cloned into the *AgeI-EcoRI* site of the pLKO.1-TRC-puro lentivector (Addgene, Cambridge, MA, USA).

Influenza Virus and VSV Infection

Influenza A virus PR8 (A/PR8/H1N1) and influenza virus GFP-PR8 strains (Manicassamy et al., 2010) were obtained from Dr. Adolfo García-Sastre (Mount Sinai School of Medicine), and VSV-GFP and VSV-WT viruses were kindly provided by Dr. Sean Whelan (Harvard Medical University). Cells were infected with influenza and VSV viruses, and viral infection was determined by standard plaque assay.

Defective MLV-EGFP Pseudotyped Virus Production and Entry Assay

To generate defective MLV-EGFP pseudotyped virus coated with different viral envelopes, 293T cells were cotransfected with pQCXIP-EGFP-retrovirus-based plasmid (Clontech), together with MLV gag/pol expression vector and a viral envelope expression plasmid as previously described (Brass et al., 2009).

Confocal, Immunofluorescence Microscopy, Colocalization Analysis, and Cholesterol Quantification

A549 cells were fixed in PBS containing 4% formaldehyde, permeablized with 0.5% Triton X-100, blocked with 1% BSA, and then stained with indicated antibodies for confocal microscopy (Nikon Eclipse Ti). The Pearson's correlation coefficients of the different fluorescent signals were determined for colocalization analysis. Total-, free-, and esterified-cholesterols were measured using the Cholesterol Quantification Kit (Sigma-Aldrich, St. Louis).

Electron Microscopy

Standard protocols were used for sample preparation, transmission electron microscopy (TEM), and immunoelectron microscopy. Electron microscopy experiments were carried out at the USC/Norris Cell & Tissue Imaging Core within the Vision Research Center.

SUPPLEMENTAL INFORMATION

Supplemental Information includes six figures and Supplemental Experimental Procedures and can be found with this article online at http://dx.doi.org/10.1016/j.chom.2013.03.006.

ACKNOWLEDGMENTS

This work was partly supported by grants from the National Institutes of Health (CA082057, CA31363, CA115284, DE019085, AI073099, AI083025, and HL110609), the Global Research Laboratory Program from the National Research Foundation of Korea (K20815000001), Hastings Foundation, Fletcher Jones Foundation (to J.U.J.), and a grant from the National Institutes of Health (U54 AI057159) (to M.F.). We thank Stacy Lee for manuscript preparation. Finally, we thank all of J.U.J.'s lab members for their discussions.

Received: August 24, 2012
Revised: December 4, 2012
Accepted: March 19, 2013
Published: April 17, 2013

REFERENCES

Amako, Y., Sarkeshik, A., Hotta, H., Yates, J., 3rd, and Siddiqui, A. (2009). Role of oxysterol binding protein in hepatitis C virus infection. J. Virol. *83*, 9237–9246.

Bailey, C.C., Huang, I.C., Kam, C., and Farzan, M. (2012). Ifitm3 limits the severity of acute influenza in mice. PLoS Pathog. *8*, e1002909.

Brass, A.L., Huang, I.C., Benita, Y., John, S.P., Krishnan, M.N., Feeley, E.M., Ryan, B.J., Weyer, J.L., van der Weyden, L., Fikrig, E., et al. (2009). The IFITM proteins mediate cellular resistance to influenza A H1N1 virus, West Nile virus, and dengue virus. Cell *139*, 1243–1254.

Carette, J.E., Raaben, M., Wong, A.C., Herbert, A.S., Obernosterer, G., Mulherkar, N., Kuehne, A.I., Kranzusch, P.J., Griffin, A.M., Ruthel, G., et al. (2011). Ebola virus entry requires the cholesterol transporter Niemann-Pick C1. Nature *477*, 340–343.

Chang, T.H., Segovia, J., Sabbah, A., Mgbemena, V., and Bose, S. (2012). Cholesterol-rich lipid rafts are required for release of infectious human respiratory syncytial virus particles. Virology *422*, 205–213.

Chernomordik, L.V., Leikina, E., Frolov, V., Bronk, P., and Zimmerberg, J. (1997). An early stage of membrane fusion mediated by the low pH conformation of influenza hemagglutinin depends upon membrane lipids. J. Cell Biol. *136*, 81–93.

Chevallier, J., Chamoun, Z., Jiang, G., Prestwich, G., Sakai, N., Matile, S., Parton, R.G., and Gruenberg, J. (2008). Lysobisphosphatidic acid controls endosomal cholesterol levels. J. Biol. Chem. *283*, 27871–27880.

Côté, M., Misasi, J., Ren, T., Bruchez, A., Lee, K., Filone, C.M., Hensley, L., Li, Q., Ory, D., Chandran, K., and Cunningham, J. (2011). Small molecule inhibitors reveal Niemann-Pick C1 is essential for Ebola virus infection. Nature *477*, 344–348.

Danthi, P., and Chow, M. (2004). Cholesterol removal by methyl-beta-cyclodextrin inhibits poliovirus entry. J. Virol. *78*, 33–41.

Diamond, M.S., and Farzan, M. (2013). The broad-spectrum antiviral functions of IFIT and IFITM proteins. Nat. Rev. Immunol. *13*, 46–57.

Ettayebi, K., and Hardy, M.E. (2003). Norwalk virus nonstructural protein p48 forms a complex with the SNARE regulator VAP-A and prevents cell

surface expression of vesicular stomatitis virus G protein. J. Virol. *77*, 11790–11797.

Everitt, A.R., Clare, S., Pertel, T., John, S.P., Wash, R.S., Smith, S.E., Chin, C.R., Feeley, E.M., Sims, J.S., Adams, D.J., et al.; GenISIS Investigators; MOSAIC Investigators. (2012). IFITM3 restricts the morbidity and mortality associated with influenza. Nature *484*, 519–523.

Feeley, E.M., Sims, J.S., John, S.P., Chin, C.R., Pertel, T., Chen, L.M., Gaiha, G.D., Ryan, B.J., Donis, R.O., Elledge, S.J., and Brass, A.L. (2011). IFITM3 inhibits influenza A virus infection by preventing cytosolic entry. PLoS Pathog. *7*, e1002337.

Ganley, I.G., and Pfeffer, S.R. (2006). Cholesterol accumulation sequesters Rab9 and disrupts late endosome function in NPC1-deficient cells. J. Biol. Chem. *281*, 17890–17899.

Gao, L., Aizaki, H., He, J.W., and Lai, M.M. (2004). Interactions between viral nonstructural proteins and host protein hVAP-33 mediate the formation of hepatitis C virus RNA replication complex on lipid raft. J. Virol. *78*, 3480–3488.

Gianni, T., and Campadelli-Fiume, G. (2012). αVβ3-integrin relocalizes nectin1 and routes herpes simplex virus to lipid rafts. J. Virol. *86*, 2850–2855.

Gruenberg, J. (2009). Viruses and endosome membrane dynamics. Curr. Opin. Cell Biol. *21*, 582–588.

Hamamoto, I., Nishimura, Y., Okamoto, T., Aizaki, H., Liu, M., Mori, Y., Abe, T., Suzuki, T., Lai, M.M., Miyamura, T., et al. (2005). Human VAP-B is involved in hepatitis C virus replication through interaction with NS5A and NS5B. J. Virol. *79*, 13473–13482.

Holthuis, J.C., and Levine, T.P. (2005). Lipid traffic: floppy drives and a superhighway. Nat. Rev. Mol. Cell Biol. *6*, 209–220.

Huang, I.C., Bailey, C.C., Weyer, J.L., Radoshitzky, S.R., Becker, M.M., Chiang, J.J., Brass, A.L., Ahmed, A.A., Chi, X., Dong, L., et al. (2011). Distinct patterns of IFITM-mediated restriction of filoviruses, SARS coronavirus, and influenza A virus. PLoS Pathog. *7*, e1001258.

Ikonen, E. (2008). Cellular cholesterol trafficking and compartmentalization. Nat. Rev. Mol. Cell Biol. *9*, 125–138.

Ioannou, Y.A. (2001). Multidrug permeases and subcellular cholesterol transport. Nat. Rev. Mol. Cell Biol. *2*, 657–668.

Jia, R., Pan, Q., Ding, S., Rong, L., Liu, S.L., Geng, Y., Qiao, W., and Liang, C. (2012). The N-terminal region of IFITM3 modulates its antiviral activity by regulating IFITM3 cellular localization. J. Virol. *86*, 13697–13707.

Kobayashi, T., Beuchat, M.H., Lindsay, M., Frias, S., Palmiter, R.D., Sakuraba, H., Parton, R.G., and Gruenberg, J. (1999). Late endosomal membranes rich in lysobisphosphatidic acid regulate cholesterol transport. Nat. Cell Biol. *1*, 113–118.

Kunz, S. (2009). Receptor binding and cell entry of Old World arenaviruses reveal novel aspects of virus-host interaction. Virology *387*, 245–249.

Lakadamyali, M., Rust, M.J., and Zhuang, X. (2004). Endocytosis of influenza viruses. Microbes Infect. *6*, 929–936.

Le Blanc, I., Luyet, P.P., Pons, V., Ferguson, C., Emans, N., Petiot, A., Mayran, N., Demaurex, N., Fauré, J., Sadoul, R., et al. (2005). Endosome-to-cytosol transport of viral nucleocapsids. Nat. Cell Biol. *7*, 653–664.

Lebrand, C., Corti, M., Goodson, H., Cosson, P., Cavalli, V., Mayran, N., Fauré, J., and Gruenberg, J. (2002). Late endosome motility depends on lipids via the small GTPase Rab7. EMBO J. *21*, 1289–1300.

Lev, S., Ben Halevy, D., Peretti, D., and Dahan, N. (2008). The VAP protein family: from cellular functions to motor neuron disease. Trends Cell Biol. *18*, 282–290.

Levine, T. (2004). Short-range intracellular trafficking of small molecules across endoplasmic reticulum junctions. Trends Cell Biol. *14*, 483–490.

Lu, J., Pan, Q., Rong, L., He, W., Liu, S.L., and Liang, C. (2011). The IFITM proteins inhibit HIV-1 infection. J. Virol. *85*, 2126–2137.

Mañes, S., del Real, G., and Martínez-A, C. (2003). Pathogens: raft hijackers. Nat. Rev. Immunol. *3*, 557–568.

Manicassamy, B., Manicassamy, S., Belicha-Villanueva, A., Pisanelli, G., Pulendran, B., and García-Sastre, A. (2010). Analysis of in vivo dynamics of influenza virus infection in mice using a GFP reporter virus. Proc. Natl. Acad. Sci. USA *107*, 11531–11536.

Maxfield, F.R., and Tabas, I. (2005). Role of cholesterol and lipid organization in disease. Nature *438*, 612–621.

Narita, K., Choudhury, A., Dobrenis, K., Sharma, D.K., Holicky, E.L., Marks, D.L., Walkley, S.U., and Pagano, R.E. (2005). Protein transduction of Rab9 in Niemann-Pick C cells reduces cholesterol storage. FASEB J. *19*, 1558–1560.

Pattanakitsakul, S.N., Poungsawai, J., Kanlaya, R., Sinchaikul, S., Chen, S.T., and Thongboonkerd, V. (2010). Association of Alix with late endosomal lysobisphosphatidic acid is important for dengue virus infection in human endothelial cells. J. Proteome Res. *9*, 4640–4648.

Peake, K.B., and Vance, J.E. (2010). Defective cholesterol trafficking in Niemann-Pick C-deficient cells. FEBS Lett. *584*, 2731–2739.

Poh, M.K., Shui, G., Xie, X., Shi, P.Y., Wenk, M.R., and Gu, F. (2012). U18666A, an intra-cellular cholesterol transport inhibitor, inhibits dengue virus entry and replication. Antiviral Res. *93*, 191–198.

Raychaudhuri, S., and Prinz, W.A. (2010). The diverse functions of oxysterol-binding proteins. Annu. Rev. Cell Dev. Biol. *26*, 157–177.

Rojek, J.M., and Kunz, S. (2008). Cell entry by human pathogenic arenaviruses. Cell. Microbiol. *10*, 828–835.

Roth, S.L., and Whittaker, G.R. (2011). Promotion of vesicular stomatitis virus fusion by the endosome-specific phospholipid bis(monoacylglycero)phosphate (BMP). FEBS Lett. *585*, 865–869.

Sadler, A.J., and Williams, B.R. (2008). Interferon-inducible antiviral effectors. Nat. Rev. Immunol. *8*, 559–568.

Schoggins, J.W., Wilson, S.J., Panis, M., Murphy, M.Y., Jones, C.T., Bieniasz, P., and Rice, C.M. (2011). A diverse range of gene products are effectors of the type I interferon antiviral response. Nature *472*, 481–485.

Schroeder, C. (2010). Cholesterol-binding viral proteins in virus entry and morphogenesis. Subcell. Biochem. *51*, 77–108.

Siegrist, F., Ebeling, M., and Certa, U. (2011). The small interferon-induced transmembrane genes and proteins. J. Interferon Cytokine Res. *31*, 183–197.

Sobo, K., Le Blanc, I., Luyet, P.P., Fivaz, M., Ferguson, C., Parton, R.G., Gruenberg, J., and van der Goot, F.G. (2007). Late endosomal cholesterol accumulation leads to impaired intra-endosomal trafficking. PLoS ONE *2*, e851.

Subramanian, K., and Balch, W.E. (2008). NPC1/NPC2 function as a tag team duo to mobilize cholesterol. Proc. Natl. Acad. Sci. USA *105*, 15223–15224.

Tang, Y., Leao, I.C., Coleman, E.M., Broughton, R.S., and Hildreth, J.E. (2009). Deficiency of niemann-pick type C-1 protein impairs release of human immunodeficiency virus type 1 and results in Gag accumulation in late endosomal/lysosomal compartments. J. Virol. *83*, 7982–7995.

Uchil, P., and Mothes, W. (2005). Viral entry: a detour through multivesicular bodies. Nat. Cell Biol. *7*, 641–642.

Veit, M., and Thaa, B. (2011). Association of influenza virus proteins with membrane rafts. Adv. Virol. *2011*, 370606.

Wang, W., Fu, Y.J., Zu, Y.G., Wu, N., Reichling, J., and Efferth, T. (2009). Lipid rafts play an important role in the vesicular stomatitis virus life cycle. Arch. Virol. *154*, 595–600.

Wee, Y.S., Roundy, K.M., Weis, J.J., and Weis, J.H. (2012). Interferon-inducible transmembrane proteins of the innate immune response act as membrane organizers by influencing clathrin and v-ATPase localization and function. Innate Immun. *18*, 834–845.

Weidner, J.M., Jiang, D., Pan, X.B., Chang, J., Block, T.M., and Guo, J.T. (2010). Interferon-induced cell membrane proteins, IFITM3 and tetherin, inhibit vesicular stomatitis virus infection via distinct mechanisms. J. Virol. *84*, 12646–12657.

Wyles, J.P., McMaster, C.R., and Ridgway, N.D. (2002). Vesicle-associated membrane protein-associated protein-A (VAP-A) interacts with the oxysterol-binding protein to modify export from the endoplasmic reticulum. J. Biol. Chem. *277*, 29908–29918.

Yan, N., and Chen, Z.J. (2012). Intrinsic antiviral immunity. Nat. Immunol. *13*, 214–222.

Yount, J.S., Karssemeijer, R.A., and Hang, H.C. (2012). S-palmitoylation and ubiquitination differentially regulate interferon-induced transmembrane protein 3 (IFITM3)-mediated resistance to influenza virus. J. Biol. Chem. *287*, 19631–19641.

Yount, J.S., Moltedo, B., Yang, Y.Y., Charron, G., Moran, T.M., López, C.B., and Hang, H.C. (2010). Palmitoylome profiling reveals S-palmitoylation-dependent antiviral activity of IFITM3. Nat. Chem. Biol. *6*, 610–614.

Zhang, M., Chen, L., Wang, S., and Wang, T. (2009). Rab7: roles in membrane trafficking and disease. Biosci. Rep. *29*, 193–209.

Zhang, Z., Liu, J., Li, M., Yang, H., and Zhang, C. (2012). Evolutionary dynamics of the interferon-induced transmembrane gene family in vertebrates. PLoS ONE *7*, e49265.